

KATANA: Simple Post-Training Robustness Using Test Time Augmentations

Gilad Cohen, Raja Giryes

Department of Electrical Engineering, Tel Aviv University, Tel Aviv, Israel
giladco1@mail.tau.ac.il, raja@tauex.tau.ac.il

Abstract

Although Deep Neural Networks (DNNs) achieve excellent performance on many real-world tasks, they are highly vulnerable to adversarial attacks. A leading defense against such attacks is adversarial training, a technique in which a DNN is trained to be robust to adversarial attacks by introducing adversarial noise to its input. This procedure is effective but must be done during the training phase. In this work, we propose a new simple and easy-to-use technique, KATANA, for robustifying an existing pretrained DNN without modifying its weights. For every image, we generate N randomized Test Time Augmentations (TTAs) by applying diverse color, blur, noise, and geometric transforms. Next, we utilize the DNN's logits output to train a simple random forest classifier to predict the real class label. Our strategy achieves state-of-the-art adversarial robustness on diverse attacks with minimal compromise on the natural images' classification. We test KATANA also against two adaptive white-box attacks and it shows excellent results when combined with adversarial training. Code is available in <https://github.com/giladcohen/KATANA>.

1 Introduction

Deep neural networks (DNNs) achieve cutting edge performance in many problems and tasks. Yet, it has been shown that small perturbations of the network, which in many cases are indistinguishable to a human observer, may alter completely the network output (Goodfellow, Shlens, and Szegedy 2015; Szegedy et al. 2014). This phenomenon pose a great risk when using neural networks in sensitive applications and therefore requires a lot of attention.

Many defense techniques were developed to improve DNN's robustness to adversarial attacks. Yet, over and over again, after the proposal of a new successful defense approach, a new attack was proposed that found new breeches in the DNNs (Carlini and Wagner 2017a; Tramer et al. 2020).

An example of a very common and successful strategy for improving DNN robustness is adversarial training (Goodfellow, Shlens, and Szegedy 2015; Madry et al. 2018). In this approach, adversarial examples are added in the network training process along with the regular examples. It is shown to reduce significantly the network vulnerability to attacks.

A major disadvantage of this approach and most of the other existing defense strategies is that they require retraining the network. This requires an additional computational time,

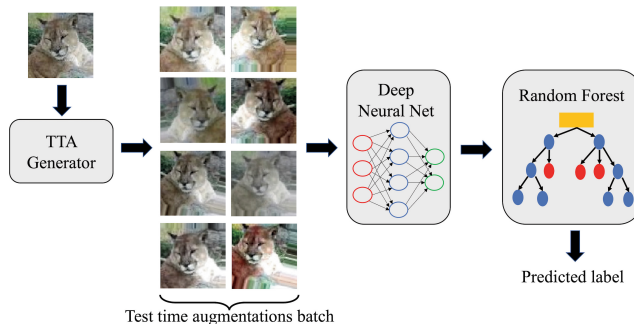


Figure 1: **KATANA flow chart.** Test time augmentations are generated and fed into a pretrained DNN. Its logits are then passed to a random forest classifier to predict the class label.

which might be significant in some cases, as one is required to update the network frequently to resist novel attacks.

Even in techniques that just fine tune the DNNs, there is a need to have an access to all the training data. The same holds also for the current leading detection methods that aim at just spotting attacks and alerting about them (without changing the DNN) (Ma et al. 2018; Lee et al. 2018; Cohen, Sapiro, and Giryes 2020). Besides storage issues, having access to all the data may be a problem when a user wants to improve its network robustness to new attacks that were not present during the development of the DNN but does not have access to the training data due to privacy or proprietary issues.

Contribution. To mitigate these issues, in this work we propose two novel approaches for improving the robustness against adversarial attacks. The first one is **Test-Time Augmentation (TTA)**, which does not require having access to the training data; The second is **Knock-out Adversaries via Test-time Augmentation Aggregation (KATANA)**, which only requires storage of logits vectors and not the images themselves. Both methods do not require retraining and can be employed with any machine learning classifier, including an adversarially trained DNN, to improve their robustness.

In both approaches, for each input image we generate N augmentations as shown in Figure 1. Our core assumption is that we may filter out the adversarial noise and predict the real class label by using many images that are slightly distinct from each other in color/orientation/noise, but se-

manically similar to the original image. While the attacks move the input into the network decision boundary that is less stable (Shamir, Melamed, and BenShmuel 2021), sampling around it is likely to return a robust prediction. The TTA classifier collects data from the DNN’s logits output (for all the TTAs), aggregates them, and selects the most probable label. KATANA does not aggregate the logits. Instead, it passes them to a random forest classifier, which is trained to be robust to logits of adversarial images.

Our methods are very simple to use, and can be applied on top of any machine learning algorithm that produces logits for an image. In addition, our techniques are fast and require only a single forward pass of the DNN in inference time (the random forest classifier inference time is negligible).

We compare our robustness strategies to state-of-the-art (SOTA) approaches for adversarial robustness against various leading attack strategies on four different datasets. We achieve improved performance in many cases using our simple proposed approaches without the need to retrain the network (the random forest training is negligible compared to a neural network training) or store the training data.

2 Related Works

Various attacks and defense techniques have been proposed for DNNs. We start by describing some of the existing attack strategies. Defense techniques may be divided into strategies that aim at increasing the network robustness and approaches that try only detecting the adversarial attacks; In this work we focus only on the former ones and describe some of them. For a more comprehensive survey of the existing strategies one may refer to (Darvish Rouani et al. 2019; Yuan et al. 2019; Miller, Xiang, and Kesidis 2020).

Adversarial attacks. The core strategy in adversarial attacks is to look for the smallest perturbation of an input that causes the network to change its prediction. The main difference between different existing attacks is the metric used to define the size of the change and the search strategy that is used for finding the perturbation. In addition, attacks may be targeted, i.e., aiming to change the output to a specific given class, or untargeted that just try to distort the network prediction. Another difference is the threat model of the attacks. Black-box adversaries can merely access the network outputs, while white-box adversaries have full access to the network architecture and parameters, algorithm used for training and classification, and training data (Chakraborty et al. 2018).

Goodfellow, Shlens, and Szegedy (2015) suggested the fast gradient sign method (FGSM) that changes the input in the direction of the gradient of the cross-entropy loss. It is a fast single-step attack that is very easy to deploy. Papernot et al. (2016) proposed the Jacobian-based saliency map attack (JSMA) that aims to find only a selected few input pixels (i.e., it uses the L_0 metric), which induce the largest loss increase, and modify only them. It is stronger but iterative and slow.

Moosavi-Dezfooli, Fawzi, and Frossard (2016) introduced Deepfool, a non-targeted attack that looks for the closest decision boundary of the network for the given input example. This approach was used also by Moosavi-Dezfooli et al. (2017) to create a universal attack, i.e., finding a perturbation that is common for multiple inputs and fool the network for

all of them. Zhang et al. (2020a) analyzed the adversarial attacks from a feature perspective and used that to propose a novel universal targeted attack.

Carlini and Wagner (2017b) proposed a novel targeted attack (known as CW due to the authors name), which was able to overcome the distillation defense method that was very successful till then (Papernot et al. 2016). Their approach was further improved by Carlini and Wagner (2017a), where they formulated an optimization framework to construct loss functions for attacks that are defense specific, i.e., adapted to specific defenses at hand. Their strategy was further improved in the Elastic-net Attack to DNNs (Chen et al. 2018) by adding an L_1 regularization to the optimization. Madry et al. (2018) showed that Projected Gradient Decent (PGD) is an optimal first order adversary, and applying it on a DNN during an adversarial training achieves optimal robustness against any first order attack.

Adversarial robustness. Many techniques were proposed to improve the adversarial robustness of DNNs.

Some techniques add a regularization during the network training; Ross and Doshi-Velez (2017) penalize the network input gradients to improve robustness. Jakubovitz and Giryes (2018) penalize the network Jacobian showing that it increases the decision boundary and thus improve robustness. Rozsa, Gunther, and E. Boulton (2018) scale the gradients in a batch based on their magnitude. Hein and Andriushchenko (2017) suggest to penalize the network output so it has a smaller Lipschitz constant. Kannan, Kurakin, and Goodfellow (2018) require similarity between logits of pairs of input examples. Cisse et al. (2017) require the linear and convolutional layers in the network to be approximately Parseval tight frames. Zhang et al. (2018, 2020b) show that the mixup regularization also improves robustness to adversarial attacks.

Other approaches rely on gradient masking (Samangouei, Kabkab, and Chellappa 2018; Dhillon et al. 2018; Buckman et al. 2018), i.e., they make it harder for attacks (especially black-box) to be able to find the gradient direction for producing the adversarial examples. Another strategy to improve robustness is adding noise to the data or perturbations to the network features during training (Jeddi et al. 2020; Xie et al. 2019; Cohen, Rosenfeld, and Kolter 2019). A different approach performs a k -NN search, perhaps using external datasets or the web, to make a decision on the input (Dubey et al. 2019; Sitawarin and Wagner 2019).

Papernot et al. (2016) proposed using network distillation to improve robustness. Chan, Tay, and Ong (2020) demonstrated that when one wishes to distill a robust network weights to another model (even with different architecture), the information of the gradients can improve the transfer.

A leading method is adversarial (re)training with its many variants (Goodfellow, Shlens, and Szegedy 2015; Madry et al. 2018; Kurakin, Goodfellow, and Bengio 2017; Tramèr et al. 2018; Shaham, Yamada, and Negahban 2018; Miyato et al. 2015; Athalye, Carlini, and Wagner 2018; Wong, Rice, and Kolter 2019). It trains the network using adversarial examples in addition to the regular data and thus improves its robustness. Carmon et al. (2019) and Zhai et al. (2019) suggested adding unlabeled data in the adversarial training to improve performance on the clean data, which is deteriorated many

times due to the adversarial training. Pang et al. (2020) improved adversarial training by using it with hyperspectral embeddings.

One of the disadvantages of many of the adversarial training methods is that they are computationally demanding. To alleviate that, Shafahi et al. (2019) suggested the “free adversarial training” approach that is fast and leads to robust networks. TRADES adds a regularization term to the cross-entropy loss in the training phase to improve robustness inside the ℓ_p ball $\mathbb{B}_p(x, \epsilon) = \{x' : \|x - x'\|_p \leq \epsilon\}$ (Zhang et al. 2019). By adjusting this term one can control the trade-off between the accuracies on the normal and adversarial samples (Stutz, Hein, and Schiele 2019). Chen et al. (2020b) and Jiang et al. (2020) showed that using robust training in the self-supervised learning regime leads to network robustness also after it is being fine-tuned for the down-stream tasks.

Notice that all of the above approaches require changing the DNN training and cannot be used for an already trained network. Indeed, one may use feature squeezing techniques that smooth or quantize the DNN input (Xu, Evans, and Qi 2018), but these methods are weaker than TRADES.

Test-time augmentation (TTA). Using image augmentations in test time was proved useful for many tasks. Sun et al. (2020) employed TTAs to improve generalization of out-of-distribution images in test time, by fine tuning the model’s parameters before making a prediction. Chen et al. (2020a) showed that extensive data augmentation as implemented by us in Section 3.1 are very useful for self-supervised learning. Qiu et al. (2020) designed FenceBox, a platform which employs 15 different data augmentation functions which are used in tandem to defend against various adversarial attacks. Their method can increase robustness for specific attacks, however, it requires a lot of manual tuning of the augmentation functions for different attacks. Our random forest classifier is trained to select features automatically for every attack. The closest work to us is (Roth, Kilcher, and Hofmann 2019). They proposed to utilize TTAs to detect adversarial images. The TTAs are used to aggregate statistics on the input image and detect anomalies associated with adversarial attacks. They showed that in some cases the correct label can also be predicted. Their approach requires an extensive statistical analysis on the dataset and tuning parameters and thresholds. Thus, it is not simple and easy to use with any arbitrary pretrained classifier as our methods.

3 Method

We turn now to present our approach. We start by describing the TTAs we generate and then showing how to use them for adversarial robustness, first for the TTA classifier and later for the KATANA classifier which uses the TTA features.

3.1 Test-time Augmentations

We hypothesize that even if the adversary succeeds to attack a specific image, the close neighborhood around the image still holds enough information for reverting the predicted attacked label back to the real, ground-truth label. To that end, for each image we generate N TTAs, using a wide variety of color, geometrical, blur, and noise transforms shown in Figure 2.

The color transforms include: Brightness, contrast, saturation, hue, and gamma; The geometric transforms include: Rotation, translation, scaling, and horizontal flipping; The blur transform convolutes the image with a 2D Gaussian kernel: $x_t = G_{2D}(u, v; \sigma_b) * x$ where x is the original image and x_t is the transformed images, and:

$$G_{2D}(u, v; \sigma_b) = \frac{1}{2\pi\sigma_b^2} \exp \frac{-(u^2 + v^2)}{2\sigma_b^2}, \quad (1)$$

where σ_b is uniformly distributed for every TTA image between 0.001 and a positive constant value σ_{bmax} :

$$\sigma_b \sim U(0.001, \sigma_{bmax}). \quad (2)$$

The noise transform adds a white Gaussian noise to the image, $x_t = x + n$, where n is sampled from:

$$n \sim N(0, \sigma), \quad (3)$$

where the standard deviation σ is uniformly distributed for every TTA image between 0 and a positive constant σ_{max} :

$$\sigma \sim U(0, \sigma_{max}). \quad (4)$$

All the transforms including their parameters are randomized in test time. More details on the transforms definitions and parameters distributions appear in the supp. mat. We chose to apply these transforms because they were shown to improve the classification accuracy significantly in self-supervised and semi-supervised learning (Chen et al. 2020a). Similarly to them, all the transforms parameters were chosen to alter the image until a human struggles to perceive the images on the dataset. We also added the Gamma transform since it showed small improvement (data not shown).

3.2 TTA Classifier

We generate N randomized TTAs and feed them to the DNN (Figure 1), we then collect their logits output (N logits vectors). Formally, for the input TTAs $\{x_t[i]\}_{i \in [0, N-1]}$, the DNN outputs are $\{l[i, c]\}_{i \in [0, N-1]}^{c \in [0, \#classes-1]}$, where $l[i, c]$ is the logit corresponding to class c of the input image $x_t[i]$.

When using only the TTAs for making the prediction, the inferred label is a simple argmax of the logits summation:

$$c_{pred} = \underset{c}{\operatorname{argmax}} \sum_{i=0}^{N-1} l[i, c]. \quad (5)$$

3.3 KATANA Classifier

We split the official test set into two: *test* and *test-val* (see Section 4 - Random forest training). Let TV be the size of *test-val*. The KATANA method employs the aforementioned DNN logits of *test-val* to train a random forest classifier. We generate N TTAs for the normal (unperturbed) images in *test-val* and additional N TTAs for adversarial images of *test-val* on a specific attack, we denote them by $\{x_t[k, i]\}$, $\{x'_t[k, i]\}_{k \in [0, TV-1], i \in [0, N-1]}$, respectively.

The above TTAs are fed to the DNN and their logits output for the normal and adversarial images are denoted as $\{l[k, i, c]\}$, $\{l'[k, i, c]\}_{k \in [0, TV-1], i \in [0, N-1]}^{c \in [0, \#classes-1]}$, respectively, or

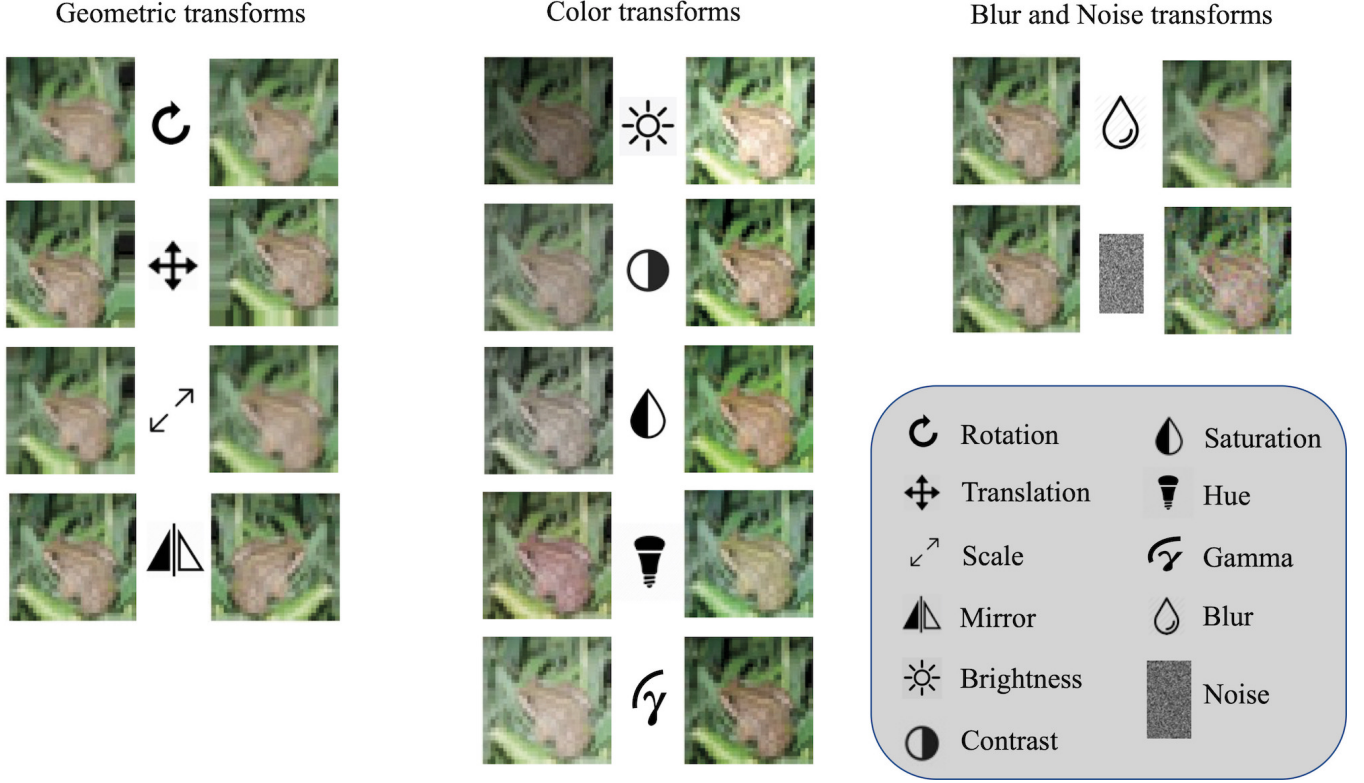


Figure 2: All the transforms used for the test-time augmentation (TTA). The left column illustrates the geometric transforms: Rotation, translation, scaling, and horizontal flips (not used on SVHN). The middle column illustrates the color transforms: Brightness, contrast, saturation, hue, and gamma. The right column illustrates a Gaussian blur and an addition of Gaussian white noise. All the above transforms are randomized to generate N TTAs samples.

$\{l[k]\}$ and $\{l'[k]\}$ in short for clarity. We then fit the random forest classifier using the pairs $\{l[k], y[k]\} \cup \{l'[k], y[k]\}$ where $y[k]$ is the true label of the image $x[k]$, i.e., it learns to infer correct labels both from regular and adversarial logits.

The random forest training procedure needs to be carried out only once. For every new (unseen) image we generate TTAs, obtain their logits $l[i, c]$ (as in Section 3.2) and feed them to the random forest classifier to predict the class label.

3.4 Adaptive Attacks

We also consider adaptive white-box threat model. In this setting the adversary knows, in addition to the model's parameters and dataset, also the exact defense algorithm. We assume that the attacker is familiar with the TTA and KATANA model schemes, but does not have access to the random forest's weights. We formulate two adaptive attacks against our methods, described below:

A-FGSM This attack applies the FGSM attack on every one of the generated TTAs in $\{x_t[i]\}_{i \in [0, N-1]}$. All the gradients are then averaged and the mean gradient map is added to the original input image. Formally, we define X_t to be the distribution of the generated TTA transforms on an image x . Given a loss function $J(x, y; w)$ where x is the input image, y is the adversarial label and w are the DNN weights, the

A-FGSM creates an adversarial image x' by:

$$\begin{aligned} x' &= x + \mathbb{E}_{x_t \sim X_t} [\epsilon \cdot \text{sign}(\nabla_{x_t} J(x_t, y; w))] \\ &= x + \frac{\epsilon}{N} \sum_{i=0}^{N-1} \text{sign}(\nabla_{x_t[i]} J(x_t[i], y; w)). \end{aligned} \quad (6)$$

A-PGD Similarly to the gradient averaging shown for A-FGSM, this adaptive attack employs the PGD attack but in every iteration we project the adversarial perturbations after the addition of the **averaged** TTAs gradients. Formally, let δ_k be the perturbation added to input image x in step k and α be the perturbation step size. The vanilla PGD attack is:

$$\delta_{k+1} = \mathcal{P} \left[\delta_k + \alpha \cdot \text{sign}(\nabla_{\delta_k} J(x + \delta_k, y; w)) \right],$$

where \mathcal{P} is the projection operator, clipping every perturbation inside a ball of interest defined by a given norm $\|\cdot\|$ (we use L_∞). For a general norm $\|\cdot\|$ it simply reads as:

$$\mathcal{P}(\delta) = \begin{cases} \frac{\delta}{\|\delta\|} \epsilon, & \text{if } \|\delta\| > \epsilon \\ \delta, & \text{otherwise.} \end{cases}$$

Our adaptive PGD attack is defined as:

$$\begin{aligned}\delta_{k+1} &= \mathcal{P} \left[\delta_k + \mathbb{E}_{x_t \sim X_t} [\alpha \cdot \text{sign}(\nabla_{\delta_k} J(x_t + \delta_k, y; w))] \right] \\ &= \mathcal{P} \left[\delta_k + \alpha \sum_{i=0}^{N-1} \text{sign}(\nabla_{\delta_k} J(x_t[i] + \delta_k, y; w)) \right],\end{aligned}\quad (7)$$

i.e., similar to PGD but averaging the gradients over the batch of augmentations. We initialize δ_0 as a zero gradient map and set the generated adversarial image as $x' = x + \delta_N$.

4 Experimental Setup

In this section we detail the datasets we used, the DNN and random forest training, the threat model used in testing, and inference computation time. Our hardware setup is thoroughly detailed in the supp. mat.

Datasets. We tested adversarial robustness on four datasets: CIFAR-10, CIFAR-100 (Krizhevsky 2009), SVHN (Netzer et al. 2011) and Tiny ImageNet (Le and Yang 2015).

DNN training. We randomly split the training set of all the datasets into two subsets, *train* and *train-val*. The former is used to back-prop gradients from the loss to the inputs and train the DNN, whereas the latter is used for metric calculation to decay the learning rate. The size of the *train-val* set is chosen to be 5% of the whole official training set.

We trained three Resnet architectures (He et al. 2016), Resnet-34, Resnet-50, and Resnet-101, with global average pooling layer before the embedding space. The embedding vector was multiplied by a fully connected layer for the logits calculation. We trained CIFAR-10, CIFAR-100, SVHN, and Tiny ImageNet with 300, 300, 200, and 300 epochs, respectively; For the TRADES method (adversarial training) we trained them with 100, 100, 100, and 300 epochs, respectively, since we observed that fewer epochs obtain higher adversarial accuracy with TRADES (see supp. mat). All TRADES adversarial robust networks were trained using $1/\lambda = 1$, $\epsilon = 0.031$, $\alpha = 0.007$ (ϵ step size), on L_∞ norm to match the settings in (Zhang et al. 2019) for fair comparison.

We use an L_2 weight decay regularization of 0.0001 in all our DNN training, a stochastic gradient decent optimizer with momentum 0.9 with Nesterov updates, and a batch size of 100. The training starts with a learning rate of 0.1, which decreases by a factor of 0.9 after 3 epochs of no improvement on the *train-val* accuracy (2 epochs for SVHN).

Random forest training. We randomly split the test set of all the datasets into two subsets, *test* and *test-val*. The *test-val* size is 2500, and the *test* is the official test set without these 2500 samples, i.e., 7500, 7500, 23500, and 7500 for CIFAR-10, CIFAR-100, SVHN, and Tiny ImageNet, respectively. The random forest classifier was trained with 1000 trees, using the Gini impurity criterion. The training time was 71 seconds and was done only once for all the normal/adversarial images on the *test* subset.

Adversarial attacks. We employed eight different adversarial attacks (norms and powers in parentheses):

1. FGSM¹: FGSM ($L_\infty, \epsilon = 0.01$)
2. FGSM²: FGSM ($L_\infty, \epsilon = 0.031$)

3. JSMA: JSMA ($L_0, \epsilon = 0.01$)
4. PGD¹: PGD ($L_\infty, \epsilon = 0.01$)
5. PGD²: PGD ($L_\infty, \epsilon = 0.031$)
6. Deepfool: Deepfool (L_2, ϵ is unconstrained)
7. CW _{L_2} : CW (L_2, ϵ is unconstrained)
8. CW _{L_∞} : CW ($L_\infty, \epsilon = 0.031$)

All attacks were implemented as targeted attacks, except of Deepfool. Our PGD attacks were used with input perturbation as shown in (Madry et al. 2018), a step size of $\alpha = 0.003$ with 100 iterations. The above attacks were selected due to their norm diversity, effectiveness, and popularity. Many attacks employ $\epsilon = 0.031$ to match the settings in the TRADES baseline (Zhang et al. 2019), which is the current SOTA.

We also employed our adaptive attacks in Section 5.3:

9. A-FGSM: A-FGSM($L_\infty, \epsilon = 0.031$)
10. A-PGD: A-PGD($L_\infty, \epsilon = 0.031$)

A-FGSM was set with $N = 256$ generated TTAs. A-PGD is very time consuming and thus was set with $N = 25$ and only 10 iterations; Thus, we updated its step size to $\alpha = 0.007$.

Testing. All the metrics we show in this work were calculated on the *test* subset. The threat model is white-box, where the adversary has full access to the model’s parameters and training data, alas the attacker is unaware that our TTA or KATANA algorithm is employed. In Section 5.3 we also consider two adaptive white-box attack, where the adversary knows our defense strategy and tries to evade it.

For both TTA and KATANA we set $N = 256$ unless stated otherwise, i.e., we generate 256 TTAs in inference time, which allows the models to run in a single forward pass on the GPU. The majority of the computation time is devoted to the TTAs generation, which is done on the CPU and takes 3.32 ± 0.33 seconds for a single Tiny ImageNet image (calculated over 20 runs). The DNN and random forest forward pass times are negligible - 250 ms and 4 ms, respectively.

5 Results

This section demonstrates the power of our TTA and KATANA classifiers against other robust methods, presents ablation studies we conducted to improve the model performance and computation time, and lastly shows accuracy on adaptive white-box attack. KATANA results using other classifiers such as logistic regression and SVM instead of the random forest are inferior and presented in the supp. mat.

Transferability. While we train here KATANA on each attack, in the supp. mat. we show its great transferability capabilities and that it can be trained on all attacks together.

5.1 Adversarial Robustness

Table 1 shows the accuracy on the normal (not attacked) datasets and the adversarial accuracies obtained for all the attacks we employed (see Section 4), on Resnet-34. Tables for Resnet-50 and Resnet-101 are shown in the supp. mat.

”Plain” corresponds to the non-robust, simple DNN accuracy, without any adversarial defense method. ”Ensemble” uses nine different DNNs with the same architecture and the predicted label is a majority voting amongst them. It should

Table 1: Comparison of accuracies (%) for various classifiers. The tested attacks and datasets are detailed in Section 4. We boldface the best results. Ensemble is presented just as a reference as it has an unfair advantage (as explained in the text).

Dataset	Method	Normal	FGSM ¹	FGSM ²	JSMA	PGD ¹	PGD ²	Deepfool	CW _{L₂}	CW _{L_∞}
CIFAR-10	Plain	94.92	68.52	55.28	68.68	13.72	0.00	4.00	3.12	23.44
	Ensemble	96.04	82.00	64.20	84.60	86.68	48.64	86.96	83.64	78.80
	TRADES	86.64	85.04	75.80	69.88	85.12	71.84	7.68	0.56	78.24
	TTA	91.68	82.48	68.76	84.84	87.04	72.76	83.16	82.24	81.4
	KATANA	93.71 ± 0.2	83.60	70.28	86.20	90.44	78.32	87.64	84.92	85.20
	TRADES + TTA	81.68	80.16	73.72	77.44	80.20	72.84	61.44	60.76	78.64
	TRADES + KATANA	83.9 ± 0.36	82.24	76.88	79.88	83.08	75.56	69.00	68.32	80.44
CIFAR-100	Plain	74.32	28.96	13.84	43.84	22.52	0.28	9.20	15.84	47.76
	Ensemble	78.04	58.20	29.16	52.48	69.64	33.28	76.60	51.08	68.68
	TRADES	53.36	51.80	41.52	46.84	52.88	46.44	10.88	5.28	51.04
	TTA	70.76	52.24	28.80	56.36	62.92	42.08	65.92	46.72	62.60
	KATANA	72.01 ± 0.45	53.60	31.12	59.88	67.08	46.88	69.04	49.80	65.24
	TRADES + TTA	50.40	48.44	43.28	48.64	49.24	44.96	45.32	35.92	49.80
	TRADES + KATANA	49.98 ± 0.59	49.88	44.28	48.16	49.52	45.96	45.68	36.04	50.96
SVHN	Plain	97.36	80.56	66.24	49.64	52.32	2.04	2.84	4.80	28.96
	Ensemble	98.12	89.52	74.84	85.36	92.80	71.20	71.88	79.76	83.04
	TRADES	92.48	90.60	81.20	39.44	90.28	70.88	5.08	0.72	82.36
	TTA	97.08	87.16	73.76	86.36	89.68	61.32	66.84	80.08	80.64
	KATANA	96.99 ± 0.15	87.76	75.84	86.84	90.24	67.36	70.64	80.44	81.24
	TRADES + TTA	89.48	88.44	80.72	78.32	88.04	77.64	55.60	45.56	82.96
	TRADES + KATANA	92.72 ± 0.49	91.56	83.00	80.92	92.12	80.56	65.48	50.76	85.72
Tiny ImageNet	Plain	59.24	25.48	9.92	28.88	30.72	0.40	10.08	16.24	34.76
	Ensemble	67.12	58.32	28.64	52.96	63.92	46.24	66.56	54.64	60.08
	TRADES	44.44	42.32	31.64	35.32	43.72	38.44	9.16	5.52	41.88
	TTA	52.48	37.12	17.36	39.76	43.84	27.52	46.24	35.08	42.96
	KATANA	54.50 ± 0.54	41.20	21.72	44.72	49.36	33.16	51.16	39.72	46.40
	TRADES + TTA	37.48	35.44	29.60	35.96	35.80	31.56	32.44	23.72	36.80
	TRADES + KATANA	39.1 ± 0.25	38.24	32.68	37.40	37.88	35.00	35.68	27.40	39.52

be emphasized that the adversary did not have access to any of these nine models. Thus, it has an unfair advantage. TTA and KATANA classifiers are shown in two setups, one is applied on a regular (non adversarially robust) DNN, and second is combined with an adversarially robust DNN trained with TRADES.

The KATANA classifier trains a different random forest model for every attack, thus, its normal test accuracy slightly differs. Therefore, for the normal accuracy we write the mean value and standard deviation over all the attacks.

We notice that for every dataset both TTA and KATANA classifiers achieve higher robustness accuracy than TRADES on JSMA, Deepfool, and CW_{L₂}. This is not surprising because TRADES employed a regularization term on a ball with an L_{∞} norm and these attacks use other norms. Nonetheless, it is not trivial that the simple TTA classifier surpasses TRADES’ accuracy on these attacks.

For the two FGSM attacks TRADES is usually better, however, we observe that in almost all cases combining TRADES with KATANA improves TRADES’ adversarial robustness on FGSM. For the low power PGD attack (PGD¹) we observe that KATANA surpasses TRADES by a large margin for CIFAR-10, CIFAR-100, and Tiny ImageNet. On SVHN they achieve comparable results.

The results on the high power PGD attack (PGD², with $\epsilon = 0.031$) are surprising because TRADES was trained with $\epsilon = 0.031$ and thus, we expect it to achieve superior adversarial accuracy (as in the FGSM² case). However, KATANA was shown to be better on CIFAR-10 and CIFAR-100.

In addition to PGD², CW_{L_∞} was also employed with an L_{∞} norm and $\epsilon = 0.031$ (matching TRADES), and still we observe that the KATANA classifier surpasses TRADES by a

large margin on CIFAR-10, CIFAR-100, and Tiny ImageNet, and achieves comparable results on SVHN.

Lastly, we observe that the normal accuracy obtained by KATANA is much better than the one of TRADES. KATANA scores almost as the “plain” classifier for normal images on CIFAR-10, CIFAR-100, and SVHN. In addition, KATANA’s normal accuracy fluctuates minimally between the attacks, as indicated by the small standard deviations.

It is interesting to point out that in many cases the “ensemble” outperforms all other methods. It is noticeable primarily for the Tiny ImageNet dataset. However, in CIFAR-10 for example, the KATANA classifier tops the “ensemble” method for every attack although the latter has an unfair advantage since the attacker has no access to its 9 networks.

5.2 Ablation Studies

We conducted two ablation studies to understand better and optimize our KATANA and TTA classifiers.

KATANA classifier ablation. For optimizing the performance of our KATANA classifier, we tested the effect of three parameters governing its accuracy:

1. Features: The inputs to the random forest classifier. We used three candidates: The DNN’s logits, the DNN’s probabilities (softmax over logits), and the embedding vectors in the DNN penultimate layer.
2. Gaussian noise power. We experimented with three different noise filters with max standard deviation (Eq. 4) of 0, 0.005, and 0.0125. The 0 value is equivalent to no noise.
3. Strength of transforms. We experimented with two sets of transforms for the transforms portrayed in Figure 2: *soft*

Table 2: Ablation study on 3 parameters used for KATANA. 1) Random forest inputs features: Logits, softmax probabilities, and DNN embeddings. 2) Randomization level of transforms: *hard* for harsh transforms and *soft* for more subtle transforms. 3) Noise transform max power (σ_{max}).

Features	Transforms	σ_{max}	Accuracy (%)	
			\mathbb{A}_{norm}	\mathbb{A}_{adv}
Logits	<i>soft</i>	0	94.24	83.56
Logits	<i>soft</i>	0.005	94.20	83.72
Logits	<i>soft</i>	0.0125	93.88	83.96
Logits	<i>hard</i>	0	93.72	84.64
Logits	<i>hard</i>	0.005	93.80	85.00
Logits	<i>hard</i>	0.0125	93.08	84.96
Probs	<i>soft</i>	0	94.16	83.36
Probs	<i>soft</i>	0.005	94.04	83.64
Probs	<i>soft</i>	0.0125	93.80	84.00
Probs	<i>hard</i>	0	93.60	84.52
Probs	<i>hard</i>	0.005	93.80	84.72
Probs	<i>hard</i>	0.0125	93.00	84.96
Embeddings	<i>soft</i>	0	94.16	83.56
Embeddings	<i>soft</i>	0.005	93.96	83.64
Embeddings	<i>soft</i>	0.0125	93.56	83.88
Embeddings	<i>hard</i>	0	93.68	84.88
Embeddings	<i>hard</i>	0.005	93.60	84.80
Embeddings	<i>hard</i>	0.0125	93.04	84.92

vs *hard*. The *soft* transforms span over shorter parameter intervals. For example, the *hard* brightness transform randomizes a brightness factor in the interval $U(0.6, 1.4)$ whereas the *soft* transform randomizes it in $U(0.8, 1.2)$. The full interval sets of the soft and hard transforms are listed in the supp. mat.

Table 2 shows the normal and adversarial accuracies (\mathbb{A}_{norm} and \mathbb{A}_{adv}) on CIFAR-10, trained by Resnet-34, and attacked by CW_{L_2} and evaluated using KATANA with $N = 1000$. The highest adversarial accuracy was obtained for logits vectors, *hard* transforms, and $\sigma_{max} = 0.005$. Thus these were the parameters we used in this work. It is interesting to point out that the best normal accuracy was obtained for *soft* transforms with $\sigma_{max} = 0$ (for all features). This observation conforms with the high normal accuracy presented in Table 1, as the plain DNN does not apply any transform.

TTA size ablation. The computational bottleneck in our TTA and KATANA classifiers is the generation of the N TTAs. Using $N = 1000$ images as done for Table 2 requires a long computation time so we searched for the minimal N , which achieves sufficient adversarial robustness. Figure 3 shows the adversarial accuracy on CIFAR-10 for three selected attacks: PGD¹, Deepfool, and CW_{L_2} in a logarithmic scale. The width of each line corresponds to the measured standard deviation of five repeated experiments. We select $N = 256$ for our experiments since it achieves good robustness with very high confidence (narrow interval). Ablation of the TTA size on CIFAR-100 and SVHN is presented in the supp. mat.

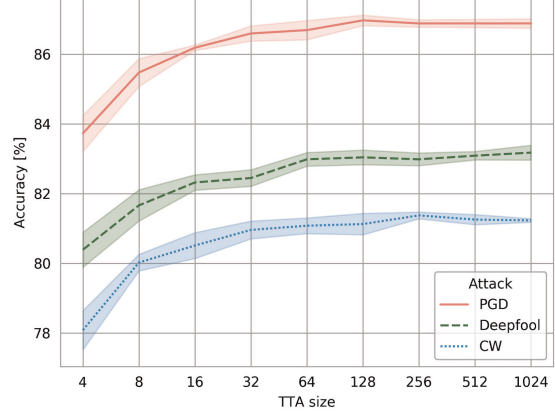


Figure 3: Ablation study on the number of generated TTAs (N). We calculate the adversarial accuracies on CIFAR-10 for three attacks as a function of N (logarithmic scale).

Table 3: Adversarial accuracies (%) for various robust classifiers on FGSM², PGD² (abbreviated to FGSM and PGD for clarity) and their adaptive counterpart A-FGSM and A-PGD. TTA and KATANA methods can maintain robustness only when combined with an adversarially trained DNN.

Dataset	Attack	Ensemble	TRADES	TTA	KATANA	TRADES+ TTA	TRADES+ KATANA
CIFAR-10	FGSM	64.20	75.80	68.76	70.28	73.72	76.88
	A-FGSM	41.60	79.20	33.32	37.80	72.96	74.88
	PGD	48.64	71.84	72.76	78.32	72.84	75.56
	A-PGD	5.76	77.76	5.12	22.32	70.40	73.24
CIFAR-100	FGSM	29.16	41.52	28.80	31.12	43.28	44.28
	A-FGSM	25.04	48.76	13.20	16.60	45.88	46.44
	PGD	33.28	46.44	42.08	46.88	44.96	45.96
	A-PGD	19.24	48.44	10.16	13.24	45.96	47.28
SVHN	FGSM	74.84	81.20	73.76	75.84	80.72	83.00
	A-FGSM	62.44	82.00	56.92	59.80	78.44	80.96
	PGD	71.20	70.88	61.32	67.36	77.64	80.56
	A-PGD	36.04	78.40	19.92	34.28	74.68	76.60
Tiny ImageNet	FGSM	28.64	31.64	17.36	21.72	29.60	32.68
	A-FGSM	30.04	40.76	6.96	10.40	31.44	35.24
	PGD	46.24	38.44	27.52	33.16	31.56	35.00
	A-PGD	38.16	40.00	6.72	10.00	33.60	35.80

5.3 Adaptive Attacks

Table 3 shows the adversarial accuracies for different robust classifiers for the vanilla FGSM²/PGD² attacks and our A-FGSM and A-PGD adaptive attacks. For all methods without an adversarially trained DNN (TRADES), we observe a substantial decrease in performance when applying the adaptive attack compared to the vanilla attack. Fortunately, combining TTA or KATANA with an adversarially trained DNN proves to be a robust classifier against the adaptive attacks.

6 Conclusion

This work proposed two simple, fast, and easy to use methods to classify adversarial images, named TTA and KATANA. Our approach is applied on pretrained DNNs without the need to carry out adversarial training or updating the model’s parameters. The TTA classifier generates many test-time augmentations, applies a wide variety of random color, geometrical, blur and noise transforms on the input image, and feed them to a pretrained DNN for classifying the correct class

label. KATANA does an extra step of passing the features collected by the TTA to a random forest classifier which yields an even better, SOTA robust classification. This improvement in robustness comes at the cost of training the random forest model (only once). Our new methods can be incorporated to work with any machine learning classifier and were shown to perform better overall when combined with an adversarially trained network. This combination was also proved to be robust against adapted white-box attacks where the adversary integrates our test-time augmentations into the attacks.

One possible future research is to apply our proposed augmentations during an adversarial training. As this may increase the training time due to the many augmentations used, in order to reduce training time, we suggest to update a SOTA DNN's parameters with this augmented adversarial training.

References

- Athalye, A.; Carlini, N.; and Wagner, D. 2018. Obfuscated gradients give a false sense of security: Circumventing defenses to adversarial examples. In *ICML*, 274–283. PMLR.
- Buckman, J.; Roy, A.; Raffel, C.; and Goodfellow, I. 2018. Thermometer Encoding: One Hot Way To Resist Adversarial Examples. In *ICLR*.
- Carlini, N.; and Wagner, D. A. 2017a. Adversarial Examples Are Not Easily Detected: Bypassing Ten Detection Methods. In *AISec@CCS*.
- Carlini, N.; and Wagner, D. A. 2017b. Towards Evaluating the Robustness of Neural Networks. *2017 IEEE Symposium on Security and Privacy (SP)*, 39–57.
- Carmon, Y.; Ragunathan, A.; Schmidt, L.; Liang, P.; and Duchi, J. C. 2019. Unlabeled Data Improves Adversarial Robustness. In *NeurIPS*.
- Chakraborty, A.; Alam, M.; Dey, V.; Chattopadhyay, A.; and Mukhopadhyay, D. 2018. Adversarial Attacks and Defences: A Survey. *ArXiv*, abs/1810.0.
- Chan, A.; Tay, Y.; and Ong, Y.-S. 2020. What It Thinks Is Important Is Important: Robustness Transfers Through Input Gradients. In *CVPR*.
- Chen, P.-Y.; Sharma, Y.; Zhang, H.; Yi, J.; and Hsieh, C.-J. 2018. EAD: Elastic-Net Attacks to Deep Neural Networks via Adversarial Examples. In *AAAI*.
- Chen, T.; Kornblith, S.; Norouzi, M.; and Hinton, G. E. 2020a. A Simple Framework for Contrastive Learning of Visual Representations. *ArXiv*, abs/2002.0.
- Chen, T.; Liu, S.; Chang, S.; Cheng, Y.; Amini, L.; and Wang, Z. 2020b. Adversarial Robustness: From Self-Supervised Pre-Training to Fine-Tuning. In *CVPR*.
- Cisse, M.; Bojanowski, P.; Grave, E.; Dauphin, Y.; and Usunier, N. 2017. Parseval Networks: Improving Robustness to Adversarial Examples. In *ICML*.
- Cohen, G.; Sapiro, G.; and Giryes, R. 2020. Detecting Adversarial Samples Using Influence Functions and Nearest Neighbors. In *CVPR*.
- Cohen, J.; Rosenfeld, E.; and Kolter, Z. 2019. Certified Adversarial Robustness via Randomized Smoothing. In *ICML*, volume 97, 1310–1320.
- Darvish Rouani, B.; Samragh, M.; Javidi, T.; and Koushanfar, F. 2019. Safe Machine Learning and Defeating Adversarial Attacks. *IEEE Security Privacy*, 17(2): 31–38.
- Dhillon, G. S.; Azizzadenesheli, K.; Bernstein, J. D.; Kossaifi, J.; Khanna, A.; Lipton, Z. C.; and Anandkumar, A. 2018. Stochastic activation pruning for robust adversarial defense. In *ICLR*.
- Dubey, A.; van der Maaten, L.; Yalniz, Z.; Li, Y.; and Mahajan, D. K. 2019. Defense Against Adversarial Images Using Web-Scale Nearest-Neighbor Search. *CVPR*, 8759–8768.
- Goodfellow, I.; Shlens, J.; and Szegedy, C. 2015. Explaining And Harnessing Adversarial Examples. In *ICLR*.
- He, K.; Zhang, X.; Ren, S.; and Sun, J. 2016. Deep Residual Learning for Image Recognition. *CVPR*, 770–778.
- Hein, M.; and Andriushchenko, M. 2017. Formal Guarantees on the Robustness of a Classifier against Adversarial Manipulation. In *NIPS*.
- Jakubovitz, D.; and Giryes, R. 2018. Improving DNN Robustness to Adversarial Attacks Using Jacobian Regularization. In *ECCV*.
- Jeddi, A.; Shafiee, M. J.; Karg, M.; Scharfenberger, C.; and Wong, A. 2020. Learn2Perturb: An End-to-End Feature Perturbation Learning to Improve Adversarial Robustness. In *CVPR*.
- Jiang, Z.; Chen, T.; Chen, T.; and Wang, Z. 2020. Robust Pre-Training by Adversarial Contrastive Learning. In *NeurIPS*.
- Kannan, H.; Kurakin, A.; and Goodfellow, I. 2018. Adversarial logit pairing. *arXiv preprint arXiv:1803.06373*.
- Krizhevsky, A. 2009. Learning multiple layers of features from tiny images. Technical report.
- Kurakin, A.; Goodfellow, I. J.; and Bengio, S. 2017. Adversarial Machine Learning at Scale. *CoRR*, abs/1611.0.
- Le, Y.; and Yang, X. 2015. Tiny ImageNet Visual Recognition Challenge.
- Lee, K.; Lee, K.; Lee, H.; and Shin, J. 2018. A simple unified framework for detecting out-of-distribution samples and adversarial attacks. *NeurIPS*, 2018-Decem: 7167–7177.
- Ma, X.; Li, B.; Wang, Y.; Erfani, S. M.; Wijewickrema, S. N. R.; Houle, M. E.; Schoenebeck, G.; Song, D.; and Bailey, J. 2018. Characterizing Adversarial Subspaces Using Local Intrinsic Dimensionality. *CoRR*, abs/1801.0.
- Madry, A.; Makelov, A.; Schmidt, L.; Tsipras, D.; and Vladu, A. 2018. Towards Deep Learning Models Resistant to Adversarial Attacks. In *ICLR*.
- Miller, D. J.; Xiang, Z.; and Kesidis, G. 2020. Adversarial Learning Targeting Deep Neural Network Classification: A Comprehensive Review of Defenses Against Attacks. *Proceedings of the IEEE*, 108(3): 402–433.
- Miyato, T.; Maeda, S.-i.; Koyama, M.; Nakae, K.; and Ishii, S. 2015. Distributional Smoothing with Virtual Adversarial Training. In *ICLR 2016*.
- Moosavi-Dezfooli, S.-M.; Fawzi, A.; Fawzi, O.; and Frossard, P. 2017. Universal Adversarial Perturbations. In *CVPR*.
- Moosavi-Dezfooli, S.-M.; Fawzi, A.; and Frossard, P. 2016. DeepFool: A simple and accurate method to fool deep neural networks. *CVPR*, 2574–2582.

- Netzer, Y.; Wang, T.; Coates, A.; Bissacco, A.; Wu, B.; and Ng, A. Y. 2011. Reading Digits in Natural Images with Unsupervised Feature Learning. In *NIPS Workshop on Deep Learning and Unsupervised Feature Learning 2011*.
- Pang, T.; Yang, X.; Dong, Y.; Xu, K.; Zhu, J.; and Su, H. 2020. Boosting Adversarial Training with Hypersphere Embedding. In *NeurIPS*.
- Papernot, N.; McDaniel, P.; Wu, X.; Jha, S.; and Swami, A. 2016. Distillation as a defense to adversarial perturbations against deep neural networks. In *IEEE Symposium on Security and Privacy (SP)*.
- Papernot, N.; McDaniel, P. D.; Jha, S.; Fredrikson, M.; Celik, Z. B.; and Swami, A. 2016. The Limitations of Deep Learning in Adversarial Settings. *2016 IEEE European Symposium on Security and Privacy (EuroS&P)*, 372–387.
- Paszke, A.; Gross, S.; Massa, F.; Lerer, A.; Bradbury, J.; Chanan, G.; Killeen, T.; Lin, Z.; Gimelshein, N.; Antiga, L.; Desmaison, A.; Kopf, A.; Yang, E.; DeVito, Z.; Raison, M.; Tejani, A.; Chilamkurthy, S.; Steiner, B.; Fang, L.; Bai, J.; and Chintala, S. 2019. PyTorch: An Imperative Style, High-Performance Deep Learning Library. In Wallach, H.; Larochelle, H.; Beygelzimer, A.; d'Alché-Buc, F.; Fox, E.; and Garnett, R., eds., *Advances in Neural Information Processing Systems 32*, 8024–8035. Curran Associates, Inc.
- Qiu, H.; Zeng, Y.; Zhang, T.; Jiang, Y.; and Qiu, M. 2020. FenceBox: A Platform for Defeating Adversarial Examples with Data Augmentation Techniques. *ArXiv*, abs/2012.0.
- Ross, A. S.; and Doshi-Velez, F. 2017. Improving the Adversarial Robustness and Interpretability of Deep Neural Networks by Regularizing Their Input Gradients. In *AAAI*.
- Roth, K.; Kilcher, Y.; and Hofmann, T. 2019. The Odds are Odd: A Statistical Test for Detecting Adversarial Examples. In *ICML*.
- Rozsa, A.; Gunther, M.; and E. Boulton, T. 2018. Towards Robust Deep Neural Networks with BANG. In *WACV*.
- Samangouei, P.; Kabkab, M.; and Chellappa, R. 2018. Defense-GAN: Protecting Classifiers Against Adversarial Attacks Using Generative Models. In *ICLR*.
- Shafahi, A.; Najibi, M.; Ghiasi, M. A.; Xu, Z.; Dickerson, J.; Studer, C.; Davis, L. S.; Taylor, G.; and Goldstein, T. 2019. Adversarial training for free! In *NeurIPS*, 3358–3369.
- Shaham, U.; Yamada, Y.; and Negahban, S. 2018. Understanding adversarial training: Increasing local stability of supervised models through robust optimization. *Neurocomputing*, 307: 195–204.
- Shamir, A.; Melamed, O.; and BenShmuel, O. 2021. The Dimpled Manifold Model of Adversarial Examples in Machine Learning. *ArXiv*, abs/2106.1.
- Sitawarin, C.; and Wágner, D. 2019. Defending Against Adversarial Examples with K-Nearest Neighbor. *ArXiv*, abs/1906.09525.
- Stutz, D.; Hein, M.; and Schiele, B. 2019. Disentangling Adversarial Robustness and Generalization. In *CVPR*.
- Sun, Y.; Wang, X.; Liu, Z.; Miller, J.; Efros, A. A.; and Hardt, M. 2020. Test-Time Training with Self-Supervision for Generalization under Distribution Shifts. In *ICML*.
- Szegedy, C.; Zaremba, W.; Sutskever, I.; Bruna, J.; Erhan, D.; Goodfellow, I.; and Fergus, R. 2014. Intriguing properties of neural networks. In *ICLR*.
- Tramer, F.; Carlini, N.; Brendel, W.; and Madry, A. 2020. On Adaptive Attacks to Adversarial Example Defenses. In *NeurIPS*.
- Tramèr, F.; Kurakin, A.; Papernot, N.; Goodfellow, I.; Boneh, D.; and McDaniel, P. 2018. Ensemble Adversarial Training: Attacks and Defenses. In *ICLR*.
- Wong, E.; Rice, L.; and Kolter, J. Z. 2019. Fast is better than free: Revisiting adversarial training. In *ICLR*.
- Xie, C.; Wu, Y.; Maaten, L. v. d.; Yuille, A. L.; and He, K. 2019. Feature denoising for improving adversarial robustness. In *CVPR*, 501–509.
- Xu, W.; Evans, D.; and Qi, Y. 2018. Feature Squeezing: Detecting Adversarial Examples in Deep Neural Networks. *CoRR*, abs/1704.0.
- Yuan, X.; He, P.; Zhu, Q.; and Li, X. 2019. Adversarial Examples: Attacks and Defenses for Deep Learning. *IEEE Transactions on Neural Networks and Learning Systems*, 30(9): 2805–2824.
- Zhai, R.; Cai, T.; He, D.; Dan, C.; He, K.; Hopcroft, J.; and Wang, L. 2019. Adversarially robust generalization just requires more unlabeled data. *arXiv preprint arXiv:1906.00555*.
- Zhang, C.; Benz, P.; Imtiaz, T.; and Kweon, I. S. 2020a. Understanding Adversarial Examples From the Mutual Influence of Images and Perturbations. In *CVPR*.
- Zhang, H.; Cissé, M.; Dauphin, Y. N.; and Lopez-Paz, D. 2018. mixup: Beyond Empirical Risk Minimization. In *ICLR*.
- Zhang, H.; Yu, Y.; Jiao, J.; Xing, E.; Ghaoui, L.; and Jordan, M. I. 2019. Theoretically Principled Trade-off between Robustness and Accuracy. In *ICML*.
- Zhang, L.; Deng, Z.; Kawaguchi, K.; Ghorbani, A.; and Zou, J. 2020b. How Does Mixup Help With Robustness and Generalization? *arXiv preprint arXiv:2010.04819*.

A Test-time Augmentations

Here we detail all the transforms we used to generate our Test-Time Augmentations (TTAs) for our robust classification methods, as described in Section 3.1 in the main paper. We used different parameters for *soft* transforms and *hard* transforms in the ablation study in Section 5.2. Both sets of parameters are listed below. The main result in the paper, outside the aforementioned ablation study, were calculated only with the *hard* set, which proved to achieve better performance in the ablation study. We denote the original and transformed images as x and x_t , respectively.

1. Rotation: Angle rotation of the image was randomized to be in $U(-8^\circ, 8^\circ)$ for *soft* and $U(-15^\circ, 15^\circ)$ for *hard*.
2. Translation: The image was allowed to shift horizontally and vertically up to 2 pixels in every direction for CIFAR-10, CIFAR-100, and SVHN, and up to 4 pixels for Tiny ImageNet. This transform behaves similarly for both *soft* and *hard*.
3. Scale: We randomly selected a zoom in ($s > 1$) or a zoom out ($s < 1$). The image was scaled with $s \sim U(0.95, 1.05)$ for *soft* and $s \sim U(0.9, 1.1)$ for *hard*.
4. Mirror: The image was horizontally flipped with a probability of 0.5. This transform was omitted for SVHN dataset, and was the same for *soft* and *hard*.
5. Brightness: Randomly increase/decrease brightness. Let b denote the brightness factor; The transforms is defined as $x_t = b \cdot x$. We randomized $b \sim U(0.8, 1.2)$ for *soft* and $b \sim U(0.6, 1.4)$ for *hard*.
6. Contrast: The contrast factor c was distributed as $c \sim U(0.85, 1.15)$ for *soft* and as $c \sim U(0.7, 1.3)$ for *hard*. The transformed image after contrast is: $x_t = c \cdot x + (1 - c) \cdot \mathbb{E}(x_G) \cdot \mathbb{1}_{n \times n \times 3}$, where $\mathbb{E}(x_G)$ is the mean pixel value on the gray-scale equivalent image and $\mathbb{1}_{n \times n \times 3}$ is a matrix as the size of the original image, filled with ones. The gray-scale image is defined as: $x_G = 0.2989 \cdot R + 0.587 \cdot G + 0.114 \cdot B$ where (R, G, B) are the red, green, and blue channels of x , respectively.
7. Saturation: The saturation factor sat was distributed as $sat \sim U(0.75, 1.25)$ for *soft* and as $sat \sim U(0.5, 1.5)$ for *hard*. It is defined as: $x_t = sat \cdot x + (1 - sat) \cdot x_G$.
8. Hue: The hue factor h was distributed as $h \sim U(0.03, 0.03)$ for *soft* and as $h \sim U(0.06, 0.06)$ for *hard*. The transform updates the hue in the Hue Saturation Value (HSV) representation by h .
9. Gamma: Applying gamma transform on the image. Each channel (r,g,b) on x is transformed to $x_t[r, g, b] = x[r, g, b]^\gamma$, where $\gamma \sim U(0.85, 1.15)$ for *soft* and $\gamma \sim U(0.7, 1.3)$ for *hard*.
10. Blur: The blur transform convolutes the image with a 2D Gaussian kernel: $x_t = G_{2D}(u, v; \sigma_b) * x$, where $G_{2D}(u, v; \sigma_b) = \frac{1}{2\pi\sigma_b^2} \exp \frac{-(u^2+v^2)}{2\sigma_b^2}$, where σ_b is uniformly distributed between 0.001 and a positive constant value σ_{bmax} : $\sigma_b \sim U(0.001, \sigma_{bmax})$.
We set $\sigma_{bmax} = 0.25$ for *soft* and $\sigma_{bmax} = 0.5$ for *hard*.
11. Noise: The Noise transform adds a white Gaussian noise to the image, $x_t = x + n$, where n is sampled from $n \sim N(0, \sigma)$. The standard deviation of the normal distribution is randomized in our algorithm to be $\sigma \sim U(0, \sigma_{max})$. We set $\sigma_{max} = 0.005$ in all our experiments (see Section 5.2 in the main paper).

It is important to point out that for all the color transforms, geometric transforms (except Mirror) and Noise, the mean value of the transform change is zero, thus our generated TTAs are unbiased.

The transforms were carried out in the following order:

- A) Applying all the color transforms ([5]-[9]). The order of the color transforms was randomized.
- B) Padding the image with the last value at the edge of the image. CIFAR-10, CIFAR-100, and SVHN were padded to 64x64x3 and Tiny ImageNet was padded to 128x128x3.
- C) Applying the random affine transform (transforms [1]-[3]).
- D) Blurring the image ([10]).
- E) Cropping the center of the image.
- F) Applying random horizontal flip (not for SVHN) ([4]).
- G) Adding noise ([11]).

Some of our transforms were implemented using the TorchVision package of PyTorch (Paszke et al. 2019).

B Hardware Setup

We trained our Deep Neural Networks (DNNs), Resnet-34, Resnet-50, and Resnet-101, with a GPU of type NVIDIA GeForce RTX 2080 Ti. This GPU has 11 GB of VRAM. We used multi workers setup and utilized 4 threads of Intel Xeon Silver 4114 CPU.

All the adversarial training with TRADES (Zhang et al. 2019) required more memory, therefore these DNNs were trained on a different server using NVIDIA RTX A6000 GPU that has 48 GB of VRAM. For training with TRADES we used 4 threads of Intel Xeon Gold 5220R CPU.

All the attacks listed in Section 4 in the paper, including the adapted attacks, were carried out on a single NVIDIA GeForce RTX 2080 Ti GPU. All the DNNs training, adversarial attacks, and evaluations were done using a single GPU.

The TTAs were generated on the CPU alone. After generated them, we fed them to the DNNs with a single forward pass (of 256 TTAs).

The random forest classifier was trained using 20 threads of Intel Xeon Silver 4114 CPU.

C Adversarial Training

We trained some TRADES models for fewer train epochs since we observed this yields more robust classifiers. The normal and adversarial accuracies on CIFAR-10, CIFAR-100, SVHN, and Tiny ImageNet trained on Resnet-34 using TRADES, is shown in Table C1. The attacks listed in the table are $\text{PGD}(L_\infty, \epsilon = 0.01)$, $\text{PGD}(L_\infty, \epsilon = 0.031)$, and $\text{CW}(L_\infty, \epsilon = 0.031)$ attacks defined in Section 4 in the main paper, abbreviated to PGD^1 , PGD^2 , and CW_{L_∞} , respectively.

Table C1: Normal and adversarial accuracies (%) for adversarially robust DNNs trained with TRADES on Resnet-34, for various number of epochs.

Dataset	Epochs	Normal	PGD^1	PGD^2	CW_{L_∞}
CIFAR-10	100	86.68	85.12	71.88	78.28
	200	87.08	84.00	67.96	74.36
	300	86.92	84.28	68.92	75.12
CIFAR-100	100	53.36	52.88	46.44	51.04
	200	53.00	52.00	47.28	50.20
	300	53.00	52.32	47.16	50.04
SVHN	100	92.48	90.28	70.88	82.36
	200	91.64	84.64	41.04	56.16
Tiny ImageNet	100	41.68	41.04	37.48	40.20
	200	43.88	43.08	37.96	42.60
	300	44.44	43.72	38.44	41.88

Based on these results we trained all the adversarial robust TRADES DNN with 100, 100, 100, and 300 epochs for CIFAR-10, CIFAR-100, SVHN, and Tiny ImageNet, respectively.

The only exception was training Tiny ImageNet on Resnet-101 with TRADES which was very time consuming, therefore we trained it only for 100 epochs instead of 300 epochs.

D Alternative Classifiers

We tested three different simple models instead of our random forest classifier in KATANA: Logistic regression, linear SVM, and SVM with an RBF kernel. Since our datasets are multi class, we set the classification strategy to be one-vs-rest. Table D1 shows results of normal and adversarial accuracies on CIFAR-10, trained on Resnet-34, and attacked by PGD¹, PGD², CW_{L₂}, and CW_{L_∞}.

Table D1: Normal and adversarial accuracies (%) on CIFAR-10 when training logistic regression or SVM compared to our proposed random forest classifier.

Classifier	PGD ¹		PGD ²		CW _{L₂}		CW _{L_∞}	
	\mathbb{A}_{norm}	\mathbb{A}_{adv}	\mathbb{A}_{norm}	\mathbb{A}_{adv}	\mathbb{A}_{norm}	\mathbb{A}_{adv}	\mathbb{A}_{norm}	\mathbb{A}_{adv}
Logistic regression	90.60	82.84	88.92	62.20	89.52	75.36	90.04	75.76
SVM (linear)	88.72	79.40	87.72	57.56	86.96	69.84	87.84	73.00
SVM (RBF)	93.64	90.04	93.48	78.24	93.44	84.80	93.60	85.44
Random forest	93.96	90.44	93.88	78.32	93.72	84.92	93.72	85.20

We observe that the random forest classifier achieves much better performance than the linear classifiers, and it is slightly better than SVM with RBF kernel. Since SVM with RBF has approximately the same computation run time as random forest, there is no reason to favor it over random forest.

E Robustness on Resnet-50 and Resnet-101

The main paper shows adversarial robustness results only on Resnet-34. In this section we repeat the results in Section 5.1 also for Resnet-50 and Resnet-101, shown in Table E1 and Table E2, respectively. Overall, the results on these DNNs have the same trend as in Resnet-34. For both Resnet-50 and Resnet-101, TTA and KATANA perform better than TRADES on JSMA, Deepfool, and CW_{L_2} . TRADES usually has higher robustness on FGSM attacks, as we observe also for Resnet-34. However, in most of these cases we notice that combination of KATANA with TRADES yields higher adversarial accuracy, as seen also for Resnet-34. Lastly, we observe that the high normal accuracy (for unperturbed images) is maintained for deeper networks.

Table E1: Comparison of accuracies (%) for various classifiers on CIFAR-10, CIFAR-100, SVHN, and Tiny ImageNet trained on Resnet-50. All attacks are detailed in Section 4 in the main paper. We boldface the best results. Ensemble is presented just as a reference as it has an unfair advantage.

Dataset	Method	Normal	FGSM ¹	FGSM ²	JSMA	PGD ¹	PGD ²	Deepfool	CW_{L_2}	CW_{L_∞}
CIFAR-10	Plain	94.80	59.12	40.00	76.24	8.16	0.00	3.44	0.08	16.00
	Ensemble	95.92	78.04	53.00	86.48	79.84	22.00	93.56	85.92	79.48
	TRADES	86.56	84.40	75.44	71.72	84.52	70.68	8.36	0.24	78.40
	TTA	90.80	78.64	59.92	84.64	83.52	57.08	87.36	82.80	81.48
	KATANA	93.25 \pm 0.2	81.28	63.72	86.08	82.92	62.12	91.40	86.12	86.88
	TRADES + TTA	80.48	78.04	72.72	76.64	78.64	70.00	58.76	59.24	77.28
	TRADES + KATANA	83.57 \pm 0.28	82.12	75.88	79.04	81.92	74.20	66.88	67.16	79.88
CIFAR-100	Plain	74.52	26.48	11.08	47.64	16.52	0.08	9.44	8.08	36.56
	Ensemble	78.44	53.60	23.08	56.72	64.48	32.64	76.88	53.84	62.4
	TRADES	55.08	53.92	44.60	45.92	54.08	48.64	11.08	5.52	52.64
	TTA	67.32	49.60	26.56	54.84	60.76	46.08	64.20	49.52	58.00
	KATANA	69.66 \pm 0.49	54.60	31.88	58.56	66.08	51.56	68.28	53.52	62.32
	TRADES + TTA	50.28	48.32	42.20	46.92	47.68	43.64	42.64	33.96	49.40
	TRADES + KATANA	51.26 \pm 0.61	50.44	45.16	48.04	50.00	46.16	45.88	34.96	51.44
SVHN	Plain	97.28	81.48	65.12	51.64	51.32	0.88	2.36	2.60	20.24
	Ensemble	97.88	91.32	75.28	85.48	92.92	71.28	84.8	85.72	85.92
	TRADES	93.72	92.92	89.76	52.36	92.00	77.76	4.24	0.40	89.08
	TTA	97.24	89.32	75.04	86.08	91.76	63.92	83.44	86.08	84.52
	KATANA	97.45 \pm 0.17	89.76	76.96	87.44	92.40	69.84	85.16	86.76	86.04
	TRADES + TTA	91.92	91.24	87.76	84.60	91.12	82.24	74.08	46.04	88.68
	TRADES + KATANA	93.85 \pm 0.56	93.80	90.44	85.88	93.60	84.64	75.68	52.16	91.24
Tiny ImageNet	Plain	64.16	25.68	11.68	32.92	30.60	0.08	9.52	17.28	41.60
	Ensemble	69.08	56.48	28.12	52.44	65.68	46.92	68.24	51.40	61.84
	TRADES	45.60	45.12	33.92	37.60	44.68	41.12	10.48	6.36	43.84
	TTA	51.88	36.88	19.08	40.16	43.36	30.20	45.92	33.08	42.80
	KATANA	55.61 \pm 0.40	42.04	22.68	46.00	50.00	36.52	50.76	39.48	47.56
	TRADES + TTA	38.04	36.28	30.44	35.88	36.52	32.24	32.48	24.64	37.64
	TRADES + KATANA	40.45 \pm 0.62	39.56	33.16	38.04	39.76	35.96	35.36	28.44	40.16

Table E2: Comparison of accuracies (%) for various classifiers on CIFAR-10, CIFAR-100, SVHN, and Tiny ImageNet trained on Resnet-101. All attacks are detailed in Section 4 in the main paper. We boldface the best results. Ensemble is presented just as a reference as it has an unfair advantage.

Dataset	Method	Normal	FGSM ¹	FGSM ²	JSMA	PGD ¹	PGD ²	Deepfool	CW _{L2}	CW _{L∞}
CIFAR-10	Plain	94.96	58.08	44.12	77.92	9.04	0.00	3.60	1.32	24.24
	Ensemble	96.24	78.76	55.56	87.48	77.52	14.36	93.52	83.08	81.16
	TRADES	85.04	82.76	72.80	70.20	82.88	68.08	8.56	0.16	75.08
	TTA	91.52	77.92	58.96	84.80	83.04	55.24	86.36	81.60	80.60
	KATANA	93.78 ± 0.17	81.12	64.20	86.96	87.68	61.28	90.72	83.92	86.28
	TRADES + TTA	80.04	78.36	72.16	75.44	78.40	70.00	57.28	60.68	77.24
	TRADES + KATANA	82.15 ± 0.33	81.08	75.08	77.12	80.96	73.76	65.96	67.00	78.80
CIFAR-100	Plain	75.56	33.20	17.56	53.44	16.72	0.12	9.40	13.52	46.92
	Ensemble	9.56	60.48	29.84	59.52	69.64	42.60	78.12	54.96	72.00
	TRADES	55.52	54.68	44.28	46.64	54.60	49.88	10.36	4.52	53.08
	TTA	68.48	51.16	32.60	59.04	62.12	48.16	65.16	48.96	62.16
	KATANA	70.82 ± 0.71	55.52	36.72	61.44	67.24	53.20	69.32	53.48	67.08
	TRADES + TTA	50.80	48.76	43.16	47.68	48.44	45.04	43.76	33.72	49.52
	TRADES + KATANA	50.82 ± 0.58	49.92	45.04	47.48	49.64	46.08	44.12	34.96	51.12]
SVHN	Plain	97.48	80.12	62.12	57.72	53.00	1.52	2.32	4.88	33.36
	Ensemble	98.08	90.04	72.04	87.80	92.72	64.80	84.12	83.12	88.12
	TRADES	93.52	93.12	89.32	38.88	92.40	74.12	4.60	0.68	87.92
	TTA	97.16	87.92	71.00	86.56	90.36	54.92	80.60	81.92	85.36
	KATANA	97.5 ± 0.15	88.68	72.60	88.16	91.08	68.76	82.44	82.44	86.00
	TRADES + TTA	92.36	91.84	88.36	78.68	91.28	80.96	67.84	51.92	88.28
	TRADES + KATANA	94.26 ± 0.43	93.84	90.60	81.36	93.92	82.96	73.64	56.76	91.16
Tiny ImageNet	Plain	66.56	25.88	11.76	34.48	30.44	0.24	9.08	14.56	40.60
	Ensemble	70.20	55.24	27.92	53.16	65.96	46.12	68.80	53.16	61.88
	TRADES	45.28	43.88	35.72	37.80	44.36	40.92	10.96	5.04	44.20
	TTA	54.84	39.08	19.52	43.48	46.00	29.96	49.96	34.84	44.76
	KATANA	58.02 ± 0.33	42.44	22.36	47.56	51.48	36.44	53.28	39.76	48.68
	TRADES + TTA	35.88	34.00	28.04	34.32	33.72	29.84	28.20	20.04	36.24
	TRADES + KATANA	38.60 ± 0.7	37.76	33.00	37.52	37.60	34.72	32.84	24.04	39.00

F Multi-attack Robustness and Transferability

The paper shows normal and adversarial accuracies where the random forest in KATANA was trained and tested on a specific attack. Here we demonstrate that KATANA classifier also exhibits robustness on various attacks simultaneously, without the need to retrain the random forest. In addition, we show excellent transferability from every one of the attacks FGSM, JSMA, PGD, Deepfool, and CW, to the other.

Table F1: Normal and adversarial accuracies (%) on CIFAR-10 using different setups for fitting the random forest. The first row is the method shown in the main paper, where the random forest is fitted and tested for each attack separately. The middle row shows global accuracies, upon fitting on all the attacks. The bottom row shows results for the Leave-One-Out Cross-Validation (LOOCV) method, where the tested attack is excluded from the random forest fitting.

Random forest fitting	Normal	FGSM ¹	FGSM ²	JSMA	PGD ¹	PGD ²	Deepfool	CW _{L₂}	CW _{L_∞}
Per attack	93.71 ± 0.2	83.60	70.28	86.20	90.44	78.32	87.64	84.92	85.20
Global	93.64	83.72	69.56	85.40	90.16	78.36	87.36	85.00	85.20
LOOCV	93.70 ± 0.09	83.52	69.28	84.84	90.56	77.72	87.32	84.92	85.00

Table F1 compares between three different setups of fitting and testing KATANA. The top row shows the accuracies we presented in Table 1 in the main paper, when applying KATANA on CIFAR-10 while fitting the random forest per attack. This method might require retraining the random forest for a new attack to improve its robustness.

The second row shows the accuracies on all the attacks FGSM¹, FGSM², JSMA, PGD¹, PGD², Deepfool, CW_{L₂}, and CW_{L_∞}, with a global random forest model, obtained while fitting it on all the aforementioned attacks. We observe a similar robustness over all the attacks.

The third row shows the KATANA accuracy using the Leave-One-Out Cross-Validation (LOOCV) procedure, where we fit the random forest on all the attacks except the attack we wish to test it on. For example, we calculate the adversarial accuracies on images generated by FGSM¹ and FGSM² after fitting the random forest on images generated by JSMA, PGD¹, PGD², Deepfool, CW_{L₂}, and CW_{L_∞}. Table F2 lists explicitly which attacks were used to fit the random forest for each tested attack. Since this cross-validation method fits five random forest models, the displayed normal accuracy is their calculated mean and standard deviation.

Table F2: Each row displays which attacks were employed to fit the random forest on the tested attack using the LOOCV procedure.

Tested attack	FGSM ¹	FGSM ²	JSMA	PGD ¹	PGD ²	Deepfool	CW _{L₂}	CW _{L_∞}
FGSM ¹			✓	✓	✓	✓	✓	✓
FGSM ²			✓	✓	✓	✓	✓	✓
JSMA	✓	✓		✓	✓	✓	✓	✓
PGD ¹	✓	✓	✓			✓	✓	✓
PGD ²	✓	✓	✓			✓	✓	✓
Deepfool	✓	✓	✓	✓	✓		✓	✓
CW _{L₂}	✓	✓	✓	✓	✓	✓		
CW _{L_∞}	✓	✓	✓	✓	✓	✓		

In Table F3 we repeated the same experiment also with the adversarially trained network on CIFAR-10, i.e., we combined TRADES with KATANA and applied the "global" and "LOOCV" random forest fitting methods as detailed above. For both the normal and adversarial images we observe comparable accuracies to the "per attack" method we applied in the paper.

Table F3: Normal and adversarial accuracies (%) on CIFAR-10 tested an adversarial trained network (TRADES) combined with KATANA, using the same random forest fitting techniques as described in Table F1.

Random forest fitting	Normal	FGSM ¹	FGSM ²	JSMA	PGD ¹	PGD ²	Deepfool	CW _{L₂}	CW _{L_∞}
Per attack	83.9 ± 0.36	82.24	76.88	79.88	83.08	75.56	69.00	68.32	80.44
Global	83.88	82.12	76.68	79.08	82.76	75.92	69.32	68.16	80.76
LOOCV	83.87 ± 0.13	81.68	76.60	79.00	82.80	75.68	69.16	67.72	80.20

G TTA Size Ablation

Here we repeat the TTA size ablation test in Section 5.2 for CIFAR-100 and SVHN datasets. We plot the adversarial accuracies for PGD¹, Deepfool, and CW_{L_2} in a logarithmic scale (Figure G1), and show that $N = 256$ TTAs are sufficient also for these datasets.

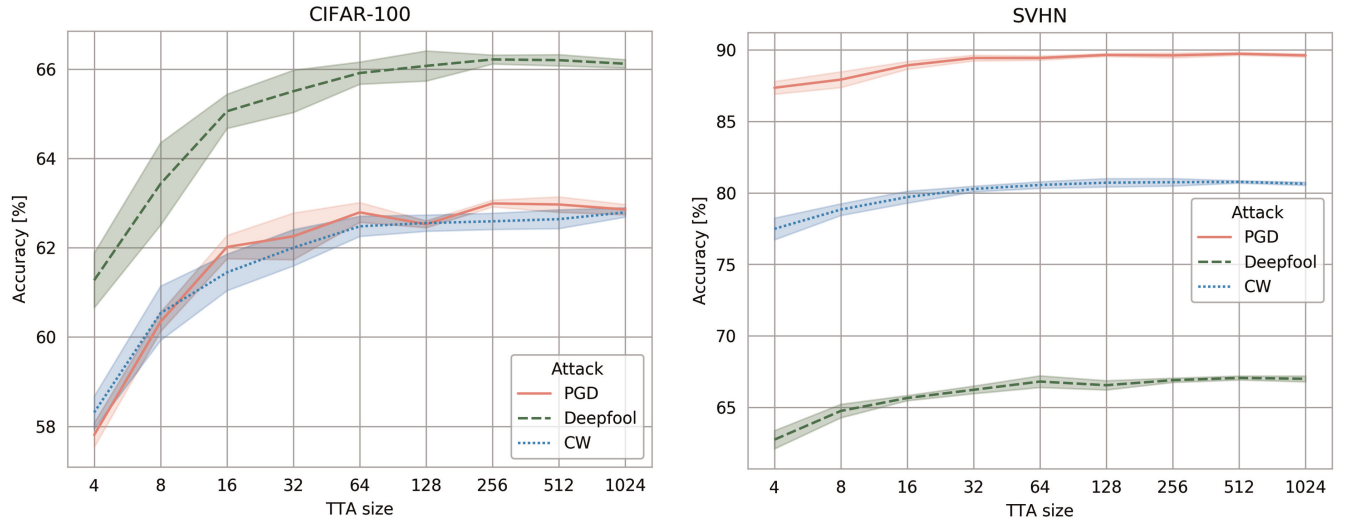


Figure G1: Ablation study on the number of generated TTAs (N). We calculate the adversarial accuracies on CIFAR-100 and SVHN for three attacks as a function of N (logarithmic scale).